Smart Structures and Systems, *Vol. 30, No. 5 (2022) 513-520*
https://doi.org/10.12989/sss.2022.30.5.513

Multi-resolution bolt preload monitoring based on the acoustoelastic effect of ultrasonic guided waves

Ruili Fu [1a], Ruiwei Mao [2b], Bo Yuan [3a], Dongdong Chen[*2] and Linsheng Huo[**4]

[1] *College of Harbour, Coastal and Offshore Engineering, Hohai University, Nanjing, Jiangsu, 210098, P.R. China*
[2] *College of Civil Engineering, Nanjing Forestry University, Nanjing, Jiangsu, 210037, P.R. China*
[3] *School of Mechanical Engineering, Dalian University of Technology, Dalian, Liaoning, 116024, P.R. China*
[4] *State Key Laboratory of Coastal and Offshore Engineering, Dalian University of Technology, Dalian, Liaoning, 116024, P.R. China*

(*Received January 14, 2022, Revised August 31, 2022, Accepted September 10, 2022*)

Abstract. During the long-time service of a bolt, its preload may suffer slight perturbations or significant reductions. It is a dilemma to monitor preload changes at high resolution and full scale. Approaches for bolt preload monitoring with multi-resolution should be developed. In this paper, a simple and effective multi-resolution bolt preload monitoring approach using ultrasonic guided waves (UGW) is proposed. A linear relationship between the time-of-flight (TOF) variation of multi-reflected waves and preload is derived to theoretically reveal the multi-resolution properties of UGW. The variations of TOF before and after the slight preload perturbations are extracted by using a global evaluation method. Experimental results show that the signal-to-noise ratio (SNR) of the 1st, 2nd, and 3rd-reflected UGWs is larger than 20 dB. The resolution of the 2nd-reflected UGW is higher than that of the 1st-reflected UGW and lower than that of the 3rd-reflected UGW. The ultimate detectable resolutions of bolt preload (DRBP) of the 1st and 3th-reflected UGWs are 0.9% and 0.5%, respectively. By using the 1st and 3th-reflected guided waves, the bolt looseness with different degrees can be monitored simultaneously.

Keywords: acoustoelastic effect; bolt preload; multi-resolution; structural health monitoring; ultrasonic guided waves

1. Introduction

As one of the commonly used connection types, bolt joints have the advantages of low cost, convenient assembly, and direct force transmission. Bolted connections are ubiquitous in mechanical (Basava and Hess 1998), aerospace (Ihn and Chang 2008), and civil engineering (Li *et al*. 2019, Que *et al*. 2019, Chen *et al*. 2020, 2022a). However, adverse diatheses, including the vibrations (Goodier and Sweeney 1945, Brøns *et al*. 2020), shocks (Hess 1998), temperature stress (Chen 2001), cyclic loads (Pai and Hess 2002a, b), et al. can cause the looseness of bolt joints. It is reported that about 20% of mechanical system failures every year worldwide are caused by the looseness of the bolt (Kaminskaya and Lipov 1990). To avoid catastrophic consequences, regular inspection and timely monitoring of bolt preload at the key joints of structures should be carried out, especially for the very early stage bolt looseness.

The prevailing inspection approaches, such as the marking and tapping methods (Zhang *et al*. 2016), highly rely on the judgment from engineering experiences, which means that these methods have much low precision and large error. In addition, the inspection process of these primary approaches is also time-consuming and laborious.

To circumvent the above-mentioned shortcomings, various technologies and methodologies have been proposed for the monitoring of bolt preload looseness (Yang *et al*. 2005, Panidis *et al*. 2013, Park *et al*. 2015, Chung and Sohn 2021). Among them, since the ultrasonic-based methods have the merits of nondestructive, good directivity, and strong penetrability (Hei *et al*. 2019), it has been widely used in the field of bolt preload monitoring (Joshi and Pathare 1984, Yang *et al*. 2019, Yasui and Kawashima 2000).

In general, ultrasonic-based methods can be divided into two categories: linear and nonlinear methods. Between them, the linear methods refer to linear characteristics of ultrasonic waves, such as amplitudes, energy dissipation, and time-of-flight (TOF). Johnson *et al*. (1986) used the TOF of both shear and longitudinal waves to measure the preload of a bolt. To simplify the monitoring process, a method that can measure the absolute preload force of a bolt was proposed by Chaki *et al*. (2007). In their study, the ratio of acoustoelastic coefficients of bi-wave (transverse and longitudinal ultrasonic waves) was defined and applied to determine the absolute preload force.

The nonlinear methods refer to the interaction between the excitation waves of different frequencies and 'breathing' type damages. For example, impact damages (Dao *et al*. 2017), fatigue cracks (Nagy 1998), and bolt preload looseness (Zhang *et al*. 2017). Nonlinear features, including

*Corresponding author, Associate Professor,
E-mail: chendongjt@163.com
**Co-corresponding author, Professor,
E-mail: lshuo@dlut.edu.cn
[a] Ph.D.
[b] Graduate Student

ISSN: 1738-1584 (Print), 1738-1991 (Online)

sub-harmonics, side-bands, and higher-order harmonics, are defined as the damage indexes to reveal the locations and degree of defects. Representatively, Pieczonka *et al*. (2018) used the modulated nonlinear vibro-acoustic waves, which are generated by pumping waves (low-frequency excitation sources) and probing waves (high-frequency excitation sources) (Pieczonka *et al*. 2015), to detect and image the shapes of the low-velocity impact damages in a composite plate.

Since the contact surfaces of bolted joints are rough and irregular, when the ultrasonic waves propagate in the bolt joints, the vibration-induced tensile and compress stresses cause the asperity contact surfaces to open and close periodically. This 'breathing' effect of bolted joints can cause nonlinear features of ultrasonic waves, which means that the frequency spectrum of output signals owns different resonant frequencies from that of the dual-frequency excitations (Zhang *et al*. 2018). Bolt preload monitoring using nonlinear acoustic techniques (NAT) has already attracted increasing attention. Nikravesh and Goudarzi (2020) investigated the efficiency of the vibro-acoustic modulation (VAM) method and the result shows that the VAM can detect bolt looseness with 12.5% precision. Three different active sensing methods, including the second harmonic, sidebands, and acoustic moments were proposed and compared by Amerini and Meo (2011). Meyer and Adams (2015) used the amplitudes of the sidebands which were excited by impact modulations to quantitatively measure the torque levels of a bolted joint. Zhang *et al*. (2016) conducted a comparative study in which the linear approach (wave energy dissipation) and nonlinear approach (e.g., VAM) were employed to demonstrate the feasibility of NAT in the detection of residual bolt torque. Literature about the investigations of NAT implies that the NAT has higher sensitivity than the linear acoustic techniques (LAT) (Sutin and Donskoy 1998, Guyer and Johnson 1999, Donskoy *et al*. 2001). However, the nonlinear VAM method usually requires three or more sensors to implement, which severely limits the scope of its application. Moreover, to actuate the 'breathing' motions, low-frequency vibration equipments, such as electro-dynamic shakers, magneto-strictive shakers, impact hammers, or stacked PZTs are needed. Therefore, the generalizability of the nonlinear VAM method remains to be further verified.

Considering that the preload of a bolt may undergo various degrees of looseness during the long-term service, approaches that can simultaneously monitor slight preload perturbation and significant preload looseness should be developed. In this paper, a simple but effective acoustoelastic-based multi-resolution bolt preload monitoring approach using ultrasonic guided waves (UGW) was proposed. The detectable resolution of bolt preload (DRBP) of multi-reflected ultrasonic guided waves is investigated (Chen *et al*. 2022b), and the change of TOF for the 1st-reflected waves, 2nd-reflected waves, and 3rd-reflected waves are measured by using a global evaluation method. The remainder of this paper is organized as follows. Section 2 is the presentation of the methodology using the acoustoelastic effect. Section 3 is the data processing technique. Experimental design and validation are carried out in Section 4. Section 5 shows the results of waveform analysis. Section 6 concludes the paper.

2. Methodology based on the acoustoelastic effect

The velocities of ultrasonic waves are related to the tensile stress of the bolt shaft which is caused by the preload force. Based on the acoustoelastic effect, for isotropic media, the velocities of ultrasonic waves can be expressed as follows (Hughes and Kelly 1953)

$$\begin{cases} \rho_0 c_{11}^2 = \lambda + 2\mu + \dfrac{\sigma_{11}}{3K_0}\left[2l + \lambda + \dfrac{\lambda+\mu}{\mu}(4m + 4\lambda + 10\mu)\right] \\ \rho_0 c_{12}^2 = \rho_0 c_{13}^2 = \mu + \dfrac{\sigma_{11}}{3K_0}\left[m + \dfrac{\lambda n}{4\mu} + 4\lambda + 4\mu\right] \\ \rho_0 c_{22}^2 = \lambda + 2\mu + \dfrac{\sigma_{11}}{3K_0}\left[2l - \dfrac{2\lambda}{\mu}(m + \lambda + 2\mu)\right] \\ \rho_0 c_{21}^2 = \mu + \dfrac{\sigma_{11}}{3K_0}\left[m + \dfrac{\lambda n}{4\mu} + \lambda + 2\mu\right] \\ \rho_0 c_{23}^2 = \mu + \dfrac{\sigma_{11}}{3K_0}\left[m - \dfrac{\lambda+\mu}{2\mu}n - 2\lambda\right] \end{cases} \tag{1}$$

where c_{ij} represents the wave velocity when the wave propagating in the direction of i (i = 1, 2) and the material polarizing in the direction of j (j = 1, 2, 3); l, m, and n are the second-order coefficients; ρ_0 is the material density at free strain; $K_0 = \lambda + 2/3\mu$ is the first-order Lame's coefficients (λ, μ); σ_{11} is the normal stress in a given media in direction 1.

When the longitudinal wave and the applied stress are in the same direction, the velocity of ultrasonic waves in Eq. (1) can be simplified as (Chaki *et al*. 2007)

$$c_{11}^{\sigma_{11}} = c_{11}^0(1 + A_{11}\sigma_{11}) \tag{2}$$

where $A_{11} = \dfrac{\lambda + 2l + \frac{(\mu+\lambda)(10\mu+4\lambda+4m)}{\mu}}{2(2\mu+\lambda)(2\mu+3\lambda)}$ is the acoustoelastic constant; $c_{11}^0 = \sqrt{\dfrac{\lambda+2\mu}{\rho_0}}$ is the wave velocity in the unstressed medium; $c_{11}^{\sigma_{11}}$ is the wave velocity corresponding to the stress of σ_{11}.

When a bolt is in the stress-free state, as shown in Fig. 1(a), the length of the bolt can be expressed as Eq. (3)

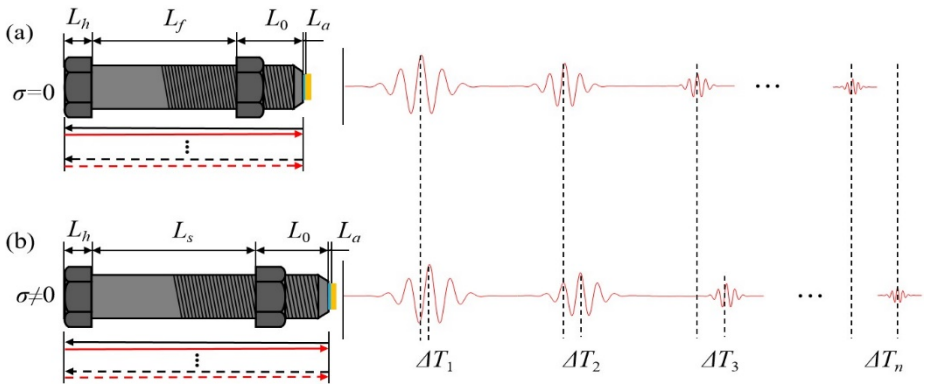

Fig. 1 Schematic diagram of ultrasonic guided waves propagating in the bolt shaft at (a) the unstressed state; and (b) the stressed state

$$L_T^{\sigma_0} = L_h + L_f + L_0 + L_a \tag{3}$$

where σ_0 represents the free stress state, $L_T^{\sigma_0}$represents the total length of the bolt in the stress-free state, L_h is the length of the bolt head, L_f is the uniaxial stress length of bolt shaft, L_0 and L_a are the unstressed length of bolt shaft, and the thickness of adhesive, respectively.

For the preload of F_1, the uniaxial stress part of the bolt shaft will elongate

$$L_s = L_f(1 + E^{-1}\sigma_1) \tag{4}$$

where E is the Young's modulus of bolt shaft, σ_1 is given by

$$\sigma_1 = \frac{F_1}{S_e^1} \tag{5}$$

S_e^1 is the effective cross-sectional area of the bolt shaft at the preload of F_1.

The length of the bolt is

$$L_T^{\sigma_1} = L_h + L_s + L_0 + L_a \tag{6}$$

For a pulse signal emitted by the surface bonded transducer, the ultrasonic wave will undergo multiple scattering and reflection in the bolt shaft and they will be recorded by the receiver. Among them, the multiple reflected waves usually have higher amplitudes and they can be used in the monitoring of bolt preload. For an ultrasonic wave passing through k times of reflection in the bolt shaft in the stress-free state, the time-of-flight is given by

$$t_k(\sigma_1) = \frac{2k(L_h + L_0)}{c_{11}^{\sigma_0}} + \frac{2kL_s}{c_{11}^{\sigma_1}} + \frac{2kL_a}{c_a} \tag{7}$$

Substituting Eqs. (4)-(6) into Eq. (7), the $t_k(\sigma_1)$ can be expressed as

$$t_k(\sigma_1) = \frac{2kL_f(1 + E^{-1}\sigma_1)}{c_{11}^{\sigma_0}(1 + A_{11}\sigma_1)} + \frac{2k(L_h + L_0)}{c_{11}^{\sigma_0}} + \frac{2kL_a}{c_a} \tag{8}$$

According to the Taylor first-order expansion, Eq. (8) can be re-written as

$$\begin{aligned} t_k(\sigma_1) &= t_k(\sigma_0) + t_k'(\sigma_0)\sigma_1 + \varsigma_1 \\ &= \frac{2k\left(L_h + L_f + L_0\right)}{c_{11}^{\sigma_0}} + \frac{2kL_a}{c_a} \\ &\quad + \frac{2kL_f(E^{-1} - A_{11})}{c_{11}^{\sigma_0}}\sigma_1 + \varsigma_1 \end{aligned} \tag{9}$$

where ζ_1 is the error of the first-order expansion.

Combining Eqs. (3) and (9) results in

$$\begin{aligned} t_k(\sigma_1) &= t_k(\sigma_0) + t_k'(\sigma_0)\sigma_1 + \varsigma_1 \\ &= \frac{2k\left(L_h + L_f + L_0\right)}{c_{11}^{\sigma_0}} + \frac{2kL_a}{c_a} \\ &\quad + \frac{2kL_f(E^{-1} - A_{11})}{c_{11}^{\sigma_0}}\frac{F_1}{S_e^1} + \varsigma_1 \end{aligned} \tag{10}$$

When a preload perturbation occurs, the transmission time of the k^{th}-reflected ultrasonic wave can be written as

$$\begin{aligned} t_k(\sigma_2) &= t_k(\sigma_0) + t_k'(\sigma_0)\sigma_2 + \varsigma_2 \\ &= \frac{2k\left(L_h + L_f + L_0\right)}{c_{11}^{\sigma_0}} + \frac{2kL_a}{c_a} \\ &\quad + \frac{2kL_f(E^{-1} - A_{11})}{c_{11}^{\sigma_0}}\frac{F_2}{S_e^2} + \varsigma_2 \end{aligned} \tag{11}$$

where S_e^2 is the effective cross-sectional area of the bolt shaft at the preload of F_2. ζ_1 is the error of the first-order expansion.

The perturbation between the two preload cases is

$$\Delta T_k = t_k(\sigma_2) - t_k(\sigma_1) \tag{12}$$

Substituting Eqs. (10)-(11) into Eq. (12) results in the new expression of ΔT_k as

$$\Delta T_k = \frac{2kL_f(E^{-1} - A_{11})}{c_{11}^{\sigma_0}}\left(\frac{F_2}{S_e^2} - \frac{F_1}{S_e^1}\right) + \varsigma_2 - \varsigma_1 \tag{13}$$

When a slight preload perturbation occurs, the change of effective cross-sectional area is neglectable

$$S_e^2 \cong S_e^1 \tag{14}$$

Eq. (13) can be rewritten as

$$\Delta T_k = \frac{2kL_f(E^{-1} - A_{11})}{c_{11}^{\sigma_0}} \Delta F + \varsigma_2 - \varsigma_1 \tag{15}$$

where $\Delta F = F_2 - F_1$.

Eq. (15) indicates that the preload varies linearly with the change of TOF. The more reflections of the ultrasonic guide wave, the greater the degree of the TOF shift.

3. Experimentation: setups, specimens, and procedures

The experimental setups include two parts: the preload simulation equipment and the signal excitation and acquisition systems. The preload simulation equipment consists of the universal test machine and the clamp. The universal test machine is applied for providing preload tension force, and the clamp is used to elongate the bolt. The data acquisition system consists of an Olympus 5077PR, a Tektronix MDO3000 oscilloscope, a PC, and the PZT transducers. In our experiment, the pulse signal emitted by Olympus 5077PR is a monocycle square wave. The transducer excitation frequency of the monocycle square wave signal is 5-6 MHz, and the peak-to-peak voltage is 400 V. In addition, the pulse repetition frequency (PRF) is set to 1 kHz. A packaged PZT transducer, as shown in Fig. 2, is pasted at the end of the bolt shaft. Firstly, polish the surface of the bolt end to be smooth. Then, clean the surface with alcohol-based sanitizers. Once the surface is dry, the epoxy adhesive is spread on the surface of the bolt end and the packaged PZT transducer is coupled. After the glue is cured for 24 hours, experimental tests can be conducted.

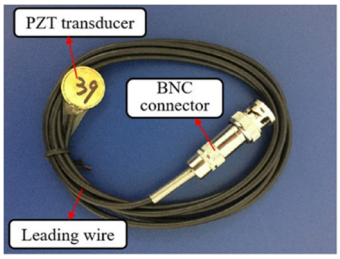

Fig. 2 Packaged PZT transducer

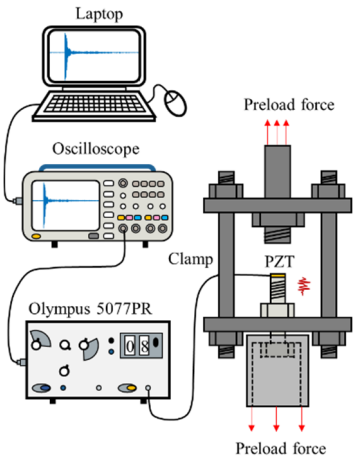

Fig. 3 Representation of the experimental setups

The PZT transducer is employed to emit and record the guided waves. The diameter and thickness of the PZT are 20 mm and 1 mm, respectively. An M20 bolt is utilized in our test. The length and the diameter of the bolt are 91.3 mm and 20 mm, respectively. The epoxy resin was used to bond the PZT with the bolt. The experiment was carried out at room temperature after the epoxy resin was cured for 24 hours. The representation of the experimental setups and the tested specimen is presented in Fig. 3.

To simulate the process of bolt looseness, four sets of unloading cases were designed, as shown in Table 1. The unloading intervals decrease with the decrease of unloading ranges. For example, the 'C2' refers to the second unloading process, which ranges from 60 kN to 30 kN. For each unloading step, the unloading interval and the unloading speeds are 30 kN and 300 N/s, respectively. The

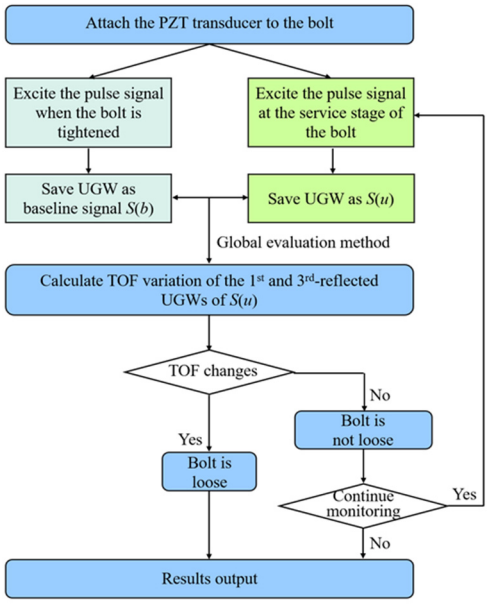

Fig. 4 Procedures of the in-situ preload monitoring using multi-reflected UGWs

Table 1 Unloading procedures

Cases	Unloading range (kN)	Unloading interval (kN)	Unloading speed (N/s)	Load holding time (s)
C1	60-0	5	500	20
C2	60-30	3	300	20
C3	60-55	0.5	50	20
C4	63-30	0.3	30	20

load holding time for all the tests is 20 s. Each test case was repeated three times.

Fig. 4 is a flowchart showing the procedures of our proposed approach. Firstly, the PZT transducer is attached to the bolt. Secondly, a pulse signal is excited when a bolt is tightened and the reflected waveform is recorded as $S(b)$. Especially for the installation stage. Thirdly, the pulse signal is excited during the service stage of the bolt and the multi-reflected UGWs are recorded as $S(u)$. Then, by using the global evaluation method, the TOF variation of the 1st and the 3rd-reflected UGWs between $S(u)$ and $S(b)$ can be obtained. If the TOF changes, which means the bolt is loose. Alternatively, the bolt is not loose, and the next monitoring step is carried out.

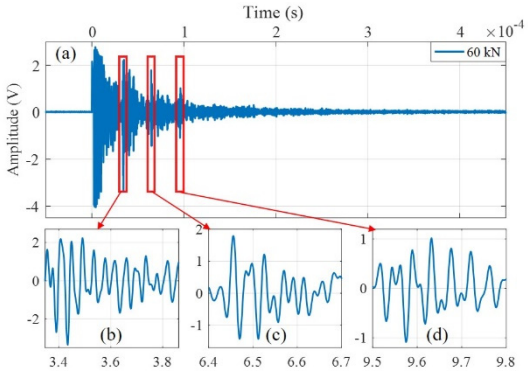

Fig. 5 Guided wave at preload of 60 kN (a) Overall waveform; (b) 1st-reflected guided wave; (c) 2nd-reflected guided wave; (d) 3rd-reflected guided wave

4. Experimental results and waveform analysis

4.1 The waveforms of multi-reflected ultrasonic guided waves

In this section, the multi-reflected ultrasonic guided waves are presented. Fig. 5 shows the waveform of the guided wave at the preload of 60 kN in the unloading case of C1. Figs. 5(b), 5(c), and 5(d) are the enlarged views of the 1st, 2nd, and 3rd-reflected guided waves of Fig. 5(a). The signal-to-noise ratio (SNR) of the 1st, 2nd, and 3rd-reflected guided waves are 27.4 dB, 25.6 dB, and 20.0 dB, respectively. For the 4th-reflected guided wave, the SNR is very low, and no apparent voltage amplitude can be found in the waveform. Therefore, the 1st, 2nd, and 3rd-reflected guided waves are extracted and analyzed for preload monitoring.

Fig. 6 shows the waveforms of the 1st, 2nd, and 3rd-reflected guided waves in the four unloading tests. Specifically, Fig. 6(a) is the 1st-reflected guided waves in the case of C1. As shown in the figure, with the decrease of preloads, the waveforms shift to the left gradually, which means that the TOF of 1st-reflected guided waves decreases with the decrease of preload. According to Eq. (15), this is mainly due to the reduction of the uniaxial stress length of

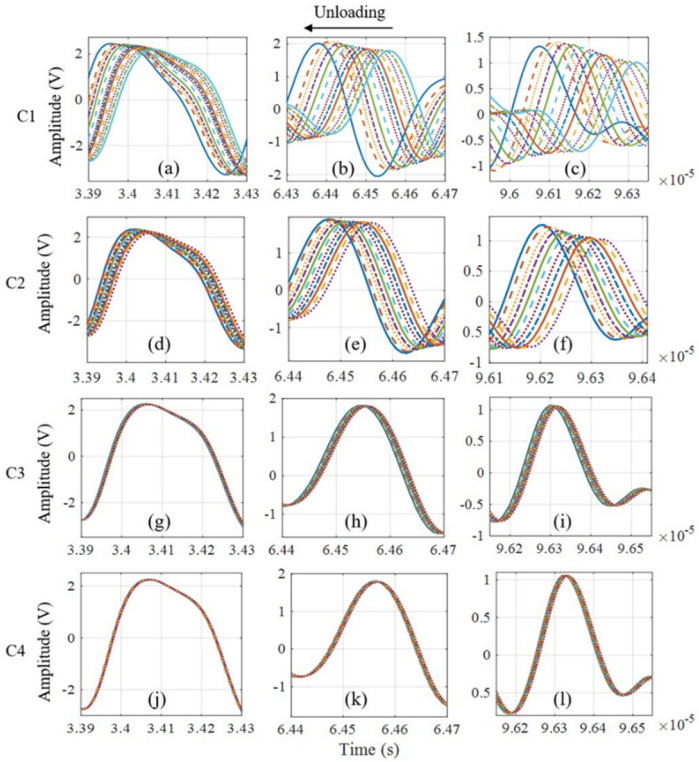

Fig. 6 Guided wave in the four unloading tests. (a) 1st-reflected UGW in C1; (b) 2nd-reflected UGW in C1; (c) 3rd-reflected UGW in C1; (d) 1st-reflected UGW in C2; (e) 2nd-reflected UGW in C2; (f) 3rd-reflected UGW in C2; (g) 1st-reflected UGW in C3; (h) 2nd-reflected UGW in C3; (i) 3rd-reflected UGW in C3; (j) 1st-reflected UGW in C4; (k) 2nd-reflected UGW in C4; (l) 3rd-reflected UGW in C4

the bolt shaft, which shortens the propagation path of the 1st-reflected guided waves. However, for the 2nd-reflected guided waves, their TOF variations are much larger than the 1st-reflected guided waves as shown in Fig. 6(b). Fig. 6(c) is the waveforms of 3rd-reflected ultrasonic waves. Compared with the 1st and 2nd-reflected guided waves, the time shifts of the 3rd-reflected ultrasonic waves are the largest. When we narrow the unloading range to 60 kN-30 kN, the waveform shifts of the 3rd-reflected ultrasonic waves are also the largest. However, the waveform shift range of the 3rd-reflected ultrasonic waves in C2 is much less than the range in C1. The same phenomena are also observed in C3 and C4. In addition, when we reduce the unloading interval from 5 kN to 0.3 kN, the TOF variations of the 1st, 2nd, and 3rd-reflected guided waves decrease as well. It should be noticed that the waveforms of the 1st-reflected guided waves overlap when the unloading interval is 0.3 kN in C4, which means that the changes of TOF are too small to reveal the preload slight perturbation. However, for the 3rd-reflected guided waves, there are slight waveform shifts in Fig. 6(i), indicating that the variations of the time-of-flight (TOF) of 3rd-reflected guided waves can be used to monitor bolt looseness. Therefore, the 1st, 2nd, and 3rd-reflected ultrasonic guided waves have different resolutions to the preload changes. The 1st-reflected UGW can function as a 'low resolution' probe to reveal the significant preload changes, and the 3rd-reflected UGW can be used as a 'high resolution' probe to sense slight preload perturbations.

4.2 The calculation of the variation of TOF

Regarding the above experimental results, the sensitivity of the 2nd-reflected UGW is higher than the 1st-reflected wave and lower than the 3rd-reflected UGW. Therefore, the 1st and 3rd-reflected UGWs are saved and extracted for the calculation of TOF.

To obtain the variations of TOF accurately, a global evaluation method is applied. In our study, three peak points of the 1st-reflected and the 3rd-reflected UGW are selected. The peak values of the three peak points are P_1^0, P_2^0, and P_3^0, and the corresponding arrival times are t_1^0,t_2^0, and t_3^0, respectively. When a preload perturbation occurs, the arrival times are t_1', t_2', and t_3', respectively.

The changes in TOF can be obtained

$$\Delta T = \frac{1}{3}\sum_{n=1}^{3}(t_n' - t_n^0) \tag{16}$$

where n = 1, 2, and 3.

Taking the 1st-reflected UGW in the case of C2-60 kN as an example, three peak values of voltage amplitudes, which are 2.212 V, 2.081 V, and 2.254 V are selected. The corresponding time points are stored for the calculation of the TOF variations, as shown in Fig. 7.

Fig. 8 shows the TOF values 1st-reflected and the 3rd-reflected UGW in the cases of C1, C2, C3, and C4. The fitting curves of the experimental results are also presented. The linear relationship between the preload changes and the changes of TOF is obtained, as shown in Eq. (17)

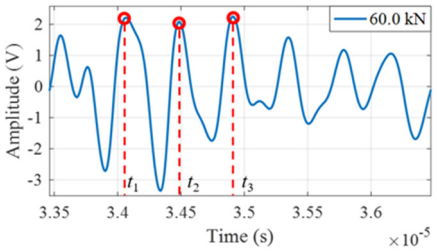

Fig. 7 Waveform of the 1st-reflected UGW in C2-60 kN

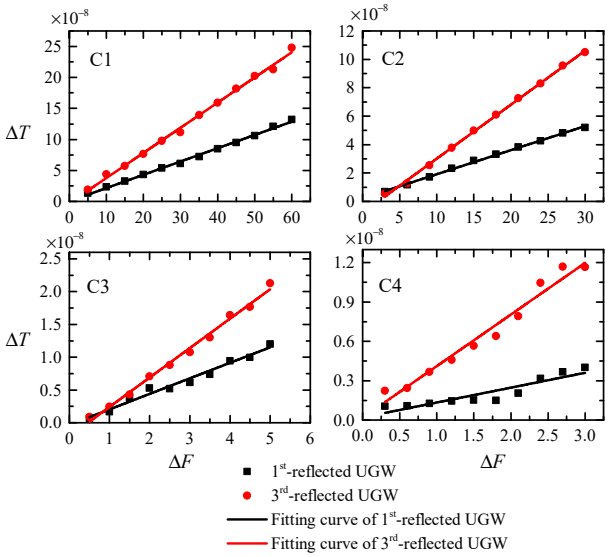

Fig. 8 Changes of TOF for the 1st-reflected and the 3rd-reflected UGWs

$$\Delta T = a + b \cdot \Delta F \tag{17}$$

where the ΔF is preload variation, ΔT represents the change of TOF. The fitting parameters in Eq. (17) are shown in Table 2.

As shown in Fig. 8 and Table 2, the preloads and the changes of TOF satisfy the linear relationship. Specifically, in the test of C1, the coefficient of determination R^2 of the 1st-reflected UGW is the same as the 3rd-reflected UGW, which is 0.966. The large value of the coefficient of determination means the high linear correlation between the variations of TOF of 1st/3rd-reflected UGW and the preload changes. For the C2, the maximum values of the changes of TOF for the 1st-reflected and the 3rd-reflected UGW are 0.052 μs and 0.105 μs, respectively. The coefficients of determination R^2 for the 1st-reflected and the 3rd-reflected UGW are larger than 0.998, which means that the TOF also changes linearly with the changes of preload. When we narrowing the preload interval to 0.5 kN, the coefficient of determination R^2 of 1st-reflected UGW is 0.966 and fluctuations occur in this case for the 1st-reflected UGW. Therefore, the changes of TOF of the 1st-reflected UGW cannot predict the preload perturbation when the unloading interval is less than 0.5 kN. For the 3rd-reflected UGW, the R^2 is 0.992, and the TOF shift linearly with the decrease of preload. Therefore, the changes of TOF of the 3rd-reflected

Table 2 Parameters of the fitting curves

Cases	UGW	a	b	R-square
C1	1st-reflected	51.91E-10	2.14E-9	0.996
	3rd-reflected	-2.70E-9	4.05E-9	0.996
C2	1st-reflected	2.23E-9	1.70E-9	0.998
	3rd-reflected	-7.83E-9	3.80E-9	0.999
C3	1st-reflected	-2.84E-10	2.31E-9	0.996
	3rd-reflected	-2.07E-9	4.49E-9	0.992
C4	1st-reflected	2.03E-10	1.13E-9	0.829
	3rd-reflected	1.83E-10	3.93E-9	0.965

UGW can function as an indicator to reveal the preload changes. However, when the unloading interval is set to 0.3 kN in C4, more fluctuations occur in the 3rd-reflected UGW, indicating that the detectable resolution of bolt preload of 3rd-reflected UGW reaches its limit.

From the above analysis, the detectable preload reductions using the 1st-reflected and the 3rd-reflected UGW are different. To quantitatively evaluate the performances of the multiply reflected ultrasonic guide wave, the detectable resolution of bolt preload (DRBP) is used. The ultimate values of DRBP of 1st-reflected and the 3rd-reflected UGW are $0.5 \cdot 2/(55.5 + 56.0) = 0.9\%$ and $0.3 \cdot 2/(60 + 60.3) = 0.5\%$, respectively. Therefore, the 3rd-reflected UGW has a higher resolution than the 1st-reflected UGW.

5. Conclusions

In this paper, a simple but novel multi-resolution bolt preload monitoring approach using UGWs is proposed. A model is built and the relationship between the variation of TOF and preload perturbation was obtained. Validation experiments were carried out and the resolution of the 1st, 2nd, and 3rd-reflected UGWs was investigated. The main findings of this paper can be drawn as follows:

- Based on the acoustoelastic effect, a theoretical model was established and the TOF varies linearly with the change of preload perturbation. In addition, the theoretical equation shows that the multi-reflected UGW owes a higher resolution than the first reflected UGW.
- Validation experiments were carried out and the results show that the 1st, 2nd, and 3rd-reflected UGWs own high levels of signal-to-noise ratio. The ultimate detectable resolution of bolt preload for the 3rd-reflected UGW is 0.5%, which is almost twice as high as that of the 1st-reflected UGW.
- The 3rd-reflected UGW is very sensitive to tiny preload changes. By using the 1st and 3th-reflected ultrasonic guided waves, the preload looseness with different degrees can be monitored simultaneously. The proposed approach holds a promising prospect for detecting preload looseness in the whole life cycle of a bolt.

Although the multi-resolution bolt preload monitoring can be achieved by using UGWs, the PZT transducer is pasted to the bolt shaft, which is inconvenient for the in-situ preload monitoring. To adopt this approach in practical applications, portable non-adhesive PZT transducers should be developed. In addition, there are a large number of bolts in a joint, and distributed sensor networks and algorithms should be investigated to detect the state and position of a loose bolt in the joint. Since the temperature changes in the outdoor environment, the influence of temperature fluctuations on waveforms shift of UGWs should be investigated, and the temperature calibration techniques will be developed in future work.

Acknowledgments

This research is financially supported by the China Postdoctoral Science Foundation (Grant No. 2022M711018), Natural Science Foundation of Jiangsu Province (Grant No. BK20220980), Jiangsu Funding Program for Excellent Postdoctoral Talent (Grant No. 2022ZB169), Fundamental Research Funds for the Central Universities (Grant No. B220201045) and the Key Laboratory of Concrete and Pre-stressed Concrete Structures of Ministry of Education (Grant No. CPCSME2022-02). The authors would like to thank for the financial supports.

References

Amerini, F. and Meo, M. (2011), "Structural health monitoring of bolted joints using linear and nonlinear acoustic/ultrasound methods", *Struct. Health Monit.*, **10**(6), 659-672. http://dx.doi.org/10.1177/1475921710395810

Basava, S. and Hess, D.P. (1998), "Bolted joint clamping force variation due to axial vibration", *J. Sound V.*, **210**(2), 255-265. https://doi.org/10.1006/jsvi.1997.1330

Brøns, M., Thomsen, J., Sah, S., Tcherniak, D. and Fidlin, A. (2020), "Analysis of transient vibrations for estimating bolted joint tightness", *Nonlinear Struc. Syst.*, **1**, 21-24. https://doi.org/10.1007/978-3-030-12391-8_3

Chaki, S., Corneloup, G., Lillamand, I. and Walaszek, H. (2007), "Combination of longitudinal and transverse ultrasonic waves for in situ control of the tightening of bolts", *J. Press. Vess. Tech-ASME.*, **129**(3), 383-390. http://dx.doi.org/10.1115/1.2748821

Chen, H.S. (2001), "The static and fatigue strength of bolted joints in composites with hygrothermal cycling", *Compos Struct.*, **52**(3-4), 295-306. https://doi.org/10.1016/S0263-8223(01)00022-8

Chen, D.D., Huo, L.S. and Song, G.B. (2020), "EMI based multi-bolt looseness detection using series/parallel multi-sensing technique", *Smart Struct. Syst., Int. J.*, **25**(4), 423-432. http://dx.doi.org/10.12989/sss.2020.25.4.423

Chen, D.D., Huo, L.S. and Song, G.B. (2022a), "High resolution bolt pre-load looseness monitoring using Coda Wave Interferometry", *Struct. Health Monit.*, **21**(5), 1959-1972. https://doi.org/10.1177/14759217211063420

Chen, D.D., Shen, Z.H., Fu, R.L., Yuan, B. and Huo, L.S. (2022b), "Coda wave interferometry-based very early stage bolt looseness monitoring using a single piezoceramic transducer", *Smart Mater. Struct.*, **31**(3), 035030. https://doi.org/10.1088/1361-665X/ac5128

Chung, J. and Sohn, H. (2021), "Detection and quantification of bolt loosening using RGB-D camera and Mask R-CNN", *Smart*

Struct. Syst., Int. J., **27**(5), 783-793. https://doi.org/10.12989/sss.2021.27.5.783

Dao, P.B., Klepka, A., Pieczonk, Ł., Aymerich, F. and Staszewsk, W.J. (2017), "Impact damage detection in smart composites using nonline-ar acoustics-cointegration analysis for removal of undesired load effect", *Smart Mater. Struct.*, **26**(3), 035012. https://doi.org/10.1088/1361-665X/aa5744

Donskoy, D., Sutin, A. and Ekimov, A. (2001), "Nonlinear acoustic interaction on contact interfaces and its use for nondestructive testing", *NDT & E Int.*, **34**(4), 231-238. https://doi.org/10.1016/S0963-8695(00)00063-3

Goodier, J.N. and Sweeney, R.J. (1945), "Loosening by vibration of threaded fastenings", *Mech. Eng.*, **67**(12), 798-802.

Guyer, R.A. and Johnson, P.A. (1999), "Nonlinear mesoscopic elasticity: evidence for a new class of materials", *Phys. Today.*, **52**(4), 30-36. https://doi.org/10.1063/1.882648

Hei, C., Luo, M., Gong, P. and Song, G. (2019), "Quantitative evaluation of bolt connection using a single piezoceramic transducer and ultrasonic coda wave energy with the consideration of the piezoceramic aging effect", *Smart Mater. Struct.*, **29**(2), 027001. https://doi.org/10.1088/1361-665X/ab6076

Hess, D.P. (1998), *Vibration- and shock-induced loosening*, Bickford J.H.; New York, NY, USA.

Hughes, D.S. and Kelly, J.L. (1953), "Second-order elastic deformation of solids", *Phys. Rev.*, **92**(5), 1145-1149. http://dx.doi.org/10.1103/PhysRev.92.1145

Ihn, J.B. and Chang, F.K. (2008), "Pitch-catch active sensing methods in structural health monitoring for aircraft structures", *Struct. Health Monit.*, **7**(1), 5-19. https://doi.org/10.1177/1475921707081979

Johnson, G.C., Holt, A.C. and Cunningham, B. (1986), "An ultrasonic method for determining axial stress in bolts", *J. Test Eval.*, **14**(5), 253-259. http://dx.doi.org/10.1520/JTE10337J

Joshi, S.G. and Pathare, R.G. (1984), "Ultrasonic instrument for measuring bolt stress" *Ultrasonics*, **22**(6), 261-269. https://doi.org/10.1016/0041-624X(84)90043-X

Kaminskaya, V. and Lipov, A. (1990), "Self loosening of bolted joints in machine tools during service", *Metal Cut Machine Tools.*, **12**, 81-85.

Kim, J.T. Nguyen, K.D. and Park, J.H. (2001), "Wireless impedance sensor node and interface washer for damage monitoring in structural connections", *Adv. Struct. Eng.*, **15**(6), 871-885. https://doi.org/10.1260/1369-4332.15.6.871

Li, H., Wang, B.J., Wei, P. and Wang, L. (2019), "Cross-laminated timber (CLT) in China: a state-of-the-art", *J. Bioresources Bioprod.*, **4**(1), 22-31. https://doi.org/10.21967/jbb.v4i1.190

Meyer, J.J. and Adams, D.E. (2015), "Theoretical and experimental evidence for using impact modulation to assess bolted joints", *Nonlinear Dynam.*, **81**(1), 103-117. http://dx.doi.org/10.1007/s11071-015-1976-6

Nagy, P.B. (1998), "Fatigue damage assessment by nonlinear ultrasonic materials characterization", *Ultrasonics.*, **36**(1-5), 375-381. https://doi.org/10.1016/S0041-624X(97)00040-1

Nikravesh, S.M.Y. and Goudarzi, M. (2020), "Experimental and numerical looseness detection and assessment in flanged joints using vibro-acoustic modulation method", *Mech. Based. Des. Struc.*, **50**(4), 1400-1416. http://dx.doi.org/10.1080/15397734.2020.1753534

Pai, N.G. and Hess, D.P. (2002a), "Experimental study of loosening of threaded fasteners due to dynamic shear loads", *J. Sound V.*, **253**(3), 585-602. https://doi.org/10.1006/jsvi.2001.4006

Pai, N.G. and Hess, D.P. (2002b), "Three-dimensional finite element analysis of threaded fastener loosening due to dynamic shear load", *Eng. Fail. Anal.*, **9**(4), 383-402. https://doi.org/10.1016/S1350-6307(01)00024-3

Panidis, T., Pavelko, I., Pavelko, V., Kuznetsov, S. and Ozolinsh, I. (2013), "Bolt-joint structural health monitoring by the method of elec-tromechanical impedance", *Aircr. Eng. Aerosp. Tec.*, **86**(3), 207-214. http://dx.doi.org/10.1108/AEAT-01-2013-0006

Park, J.H., Huynh, T.C., Choi, S.H. and Kim, J.T. (2015), "Vision-based technique for bolt-loosening detection in wind turbine tower", *Wind Struct., Int. J.*, **21**(6), 709-726. http://dx.doi.org/10.12989/was.2015.21.6.709

Pieczonka, L., Klepka, A., Martowicz, A. and Staszewski, W.J. (2015), "Nonlinear vibroacoustic wave modulations for structural damage detection: an overview", *Optical Eng.*, **55**(1), 011005. https://doi.org/10.1117/1.OE.55.1.011005

Pieczonka, L., Zietek, L., Klepka, A., Staszewski, W.J., Aymerich, F. and Uhl, T. (2018), "Damage imaging in composites using nonlinear vibro-acoustic wave modulations", *Struct. Control Health Monit.*, **25**(2), 1-13. https://doi.org/10.1002/stc.2063

Que, Z., Hou, T., Gao, Y., Teng, Q., Chen, Q., Wang, C. and Chang, C. (2019), "Influence of different connection types on mechanical behavior of girder trusses", *J. Bioresources Bioprod.*, **4** (2), 89-98. https://doi.org/10.21967/jbb.v4i2.229

Sutin, A.M. and Donskoy, D.M. (1998), "Vibro-acoustic modulation nondestructive evaluation technique", *J. Intel. Mat. Syst. Struct.*, **9**(9), 765-771. http://dx.doi.org/10.1117/12.305057

Yang, J., Liu P., Yang, S., Lee, H. and Sohn, H. (2005), "Laser based impedance measurement for pipe corrosion and bolt-loosening detection", *Smart Struct. Syst., Int. J.*, **15**(1), 41-55. https://doi.org/10.12989/sss.2015.15.1.041

Yang, Y. and Ng, C. and Kotousov, A. (2019), "Bolted joint integrity monitoring with second harmonic generated by guided waves", *Struct. Health Monit.*, **18**(1), 193-204. https://doi.org/10.1177/1475921718814399

Yasui, H. and Kawashima, K. (2000), "Acoustoelastic measurement of bolt axial load with velocity ratio method", *Proceedings of the 15th World Conference on Nondestructive Testing*, Italy, Roma, October.

Yin, H.Y., Wang, T., Yang, D., Liu, S.P., Shao, J.H. and Li, Y.R. (2016), "A smart washer for bolt looseness monitoring based on piezoelectric active sensing method", *Appl. Sci.*, **6**(11), p. 320. http://dx.doi.org/10.3390/app6110320

Zhang, L., Chen, Z., Dong, H., Fu, S., Ma, L. and Yang, X. (2001), "Wood plastic composites based wood wall;' structure and thermal insulation performance", *J. Bioresources Bioprod.*, **6**(1), 65-74. https://doi.org/10.1016/j.jobab.2021.01.005

Zhang, Z., Liu, M., Su, Z. and Xiao, Y. (2016), "Quantitative evaluation of residual torque of a loose bolt based on wave energy dissipation and vibro-acoustic modulation: a comparative study", *J. Sound V.*, **383**, 156-170. http://dx.doi.org/10.1016/j.jsv.2016.07.001

Zhang, M.Y., Shen, Y.F., Xiao, L. and Qu, W.Z. (2017), "Application of subharmonic resonance for the detection of bolted joint looseness", *Nonlinear Dynam.*, **88**(3), 1643-1653. http://dx.doi.org/10.1007/s11071-017-3336-1

Zhang, Z., Liu, M., Liao, Y., Su, Z. and Xiao, Y. (2018), "Contact acoustic nonlinearity (CAN)-based continuous monitoring of bolt loosen-ing: hybrid use of high-order harmonics and spectral sidebands", *Mech. Syst. Signal Pr.*, **103**, 280-294. https://doi.org/10.1016/j.ymssp.2017.10.009

HJ